

Nanoscale

Accepted Manuscript



This is an *Accepted Manuscript*, which has been through the Royal Society of Chemistry peer review process and has been accepted for publication.

Accepted Manuscripts are published online shortly after acceptance, before technical editing, formatting and proof reading. Using this free service, authors can make their results available to the community, in citable form, before we publish the edited article. We will replace this *Accepted Manuscript* with the edited and formatted *Advance Article* as soon as it is available.

You can find more information about *Accepted Manuscripts* in the [Information for Authors](#).

Please note that technical editing may introduce minor changes to the text and/or graphics, which may alter content. The journal's standard [Terms & Conditions](#) and the [Ethical guidelines](#) still apply. In no event shall the Royal Society of Chemistry be held responsible for any errors or omissions in this *Accepted Manuscript* or any consequences arising from the use of any information it contains.

In vivo Multimodality Imaging of miRNA-16 Iron Nanoparticle Reversing Drug Resistant to Chemotherapy in A Mouse Gastric Cancer Model

Zhongchan Sun ^{a,b,1}, Xinxing Song ^{b,c,1}, Xiujuan Li ^b, Tao Su ^b, Shun Qi ^d, Ruirui Qiao ^e, Fu Wang ^f, Yi Huan ^d,

Weidong Yang ^g, Jing Wang ^g, Yongzhan Nie ^h, Kaichun Wu ^h, Mingyuan Gao ^e, Feng Cao ^{a,b,*}

^a Department of Cardiology, Chinese PLA General Hospital, Beijing , 100853, China

^b Department of Cardiology & Molecular Imaging Program, Xijing Hospital, Fourth Military Medical University, Xi'an 710032, China

^c Department of Cardiology, 285 Hospital, Handan 056001, China

^d Department of Radiology, Xijing Hospital, Fourth Military Medical University, Xi'an 710032, China

^e Institute of Chemistry, Chinese Academy of Sciences, Bei Yi Jie 2, Zhong Guan Cun, Beijing 100190, China

^f Life Sciences Research Center, School of Life Sciences and Technology, Xidian University, Xi'an 710071, China

^g Department of Nuclear Medicine, Xijing Hospital, Fourth Military Medical University, Xi'an 710032, China

^h Department of Digestive Disease, Xijing Hospital, Fourth Military Medical University, Xi'an 710032, China

¹ These authors contributed equally to this work and should be considered as co-first authors.

* Correspondence to:

Feng Cao, MD, PhD

Department of Cardiology, Chinese PLA General Hospital, 28[#] Fuxing Street, Beijing , 100853, China

Department of Cardiology & Molecular Imaging Program, Xijing Hospital, Fourth Military Medical University,

Xi'an 710032, China

Phone: 86-29-84771024

Fax: 86-29-84775183

Email: wind8828@gmail.com

Abstract

miRNA-16 (miR16) plays an important role in modulating drug resistance of SGC7901 cell lines to adriamycin (ADR). A variety of viral carriers has been designed for miRNA delivery. However, the safety concerns are currently perceived as hamper to the clinical application of viral vector-based therapy. Herein a type of magnetic nanoparticles (MNPs) was designed and synthesized using a poly (ethylene glycol) (PEG)-coated Fe₃O₄ nanoparticles as a miRNA delivery system for the purpose of reducing drug resistance of gastric cancer cells by enforcing miR16 expression in SGC7901/ADR cells. The MNPs with good biocompatibility were synthesized by thermal decomposition and then conjugated with miRNA via electrostatic interaction, producing miR16/MNPs. After co-culture with miR16/MNPs, ADR induced apoptosis of SGC7901/ADR was examined by MTT and TUNEL. miR16/MNPs treatment significantly increased cell apoptosis *in vitro*. SGC7901/ADR^{FLuc} tumor bearing nude mice under ADR therapy were treated with miR16/MNPs by tail vein injection for *in vivo* study. After intra peritoneal injection of ADR, tumor volume measurement and fluorescence imaging were performed to assess death of SGC7901/ADR cells *in vivo*. Results showed that miR16/MNPs were able to significantly suppress SGC7901/ADR tumor growth, probably through increasing SGC7901/ADR cells sensitivity to ADR. Our results suggest the great promise of miR16 delivered by MNPs as a novel therapeutic strategy for drug resistant tumor treatment.

Key Words: drug resistance; nanoparticles; miRNA-16 (miR16); molecular imaging

Introduction

Gastric cancer is one of the most common human malignancies and the second leading cause of cancer death in the world¹. It is generally accepted that drug resistance is a major contributor to chemotherapy failure for Gastric cancer². Therefore, reversing drug resistance is a novel strategy for drug resistant tumor treatment and may enhance the effectiveness of chemotherapy.

microRNAs (miRNAs) are a well-known class of small RNAs that inhibit gene expression at the post-transcriptional level by directly targeting regions of sequence complementarity in the 3'-untranslated regions (3'-UTRs) of mRNAs. Manipulation of miRNA is considered a novel strategy for reversing drug resistance in tumor cells³. miRNA-16 (miR16) is a well-recognized tumor suppressing miRNA^{4,5} and our previous work showed miR16 was able to sensitize drug resistant gastric cancer cells by down-regulating its target protein Bcl-2, an anti-apoptotic gene, which was found to be elevated in drug resistant cells⁶. Theoretically, exogenous delivery of miR16 would sensitize drug resistant gastric cancer cells and significantly enhance the therapeutic effect of anti-tumor medication. A variety of viral carriers have been designed for miRNA delivery and have shown high transfection efficiencies over a broad range of cell types. However, the safety concerns are currently perceived as hamper to the clinical application of viral vector-based therapy.

Nanoparticles are developed as delivery platform for molecules and reagents used in human cancer diagnosis and therapy by taking advantage of their unique physicochemical property⁷⁻⁹. Due to their appropriate diameters and the enhanced permeability of tumor vasculature, nanoparticles can accumulate passively in tumor by enhanced permeability and retention (EPR) effect¹⁰. Recently, accumulating evidence also suggested that nanoparticles can function as a good delivery system for miRNA¹¹⁻¹³. Moreover, nanoparticles are able to be dynamically traced by MRI, ultrasound, and optical imaging *in vivo* owing to their own physical performance or through conjugation with

various specific labeling markers. This particular property of nanoparticles allows the determination of their fate noninvasively, which indirectly reflect the fate of their payload, making it particularly useful for evaluating the effectiveness of the delivery system *in vivo*.

Magnetic iron oxide nanoparticles (MNPs) have been widely used as a new type of magnetic resonance contrast agent for its excellent safety and biocompatibility profile¹⁴. It has been used for multiple purposes such as detection of different diseases including inflammatory and degenerative diseases, early tumor detections^{15, 16} and blood-brain barrier transport¹⁷, etc. Recently, its potential as a drug delivery system has been brought under spotlight. In the present study, we report the construction of a miRNA delivery probe by using a well-defined poly (ethylene glycol) (PEG)-coated Fe₃O₄ nanoparticle (MNPs) as both carrier and MRI contrast agent. The delivery efficiency and therapeutic effect of this particular magnetic nanoparticles-based miR16 carrier in MDR SGC7901 cells were assessed in both *in vitro* and *in vivo* models. Our results demonstrated that Fe₃O₄ nanoparticles conjugated miR16 (miR16/MNPs) can effectively deliver miR16 to SGC7901/ADR cells and increase their sensitivity to ADR.

Materials and Methods

Animals

Specific pathogen-free 8-week-old female Balb/c nude mice were obtained from the Shanghai Animal Center in China and bred in the Fourth Military Medical University animal center, China. All experimental animals were housed under specific pathogen-free conditions. The animal protocols used in this study were approved by the Fourth Military Medical University Ethics. All procedures were performed in accordance with the Fourth Military Medical University Guide for the Care and Use of Laboratory Animals formulated by the National Society for Medical Research.

Reagents and antibodies

MNPs were synthesized by a modified “one-pot” synthetic approach according to our previous reports^{18, 19}. Cy5.5 NHS ester was purchased from GE (GE Healthcare, Piscataway, N.J, USA). The miR16 and negative control (NC) RNA oligos were synthesized (Shanghai GenePharma, China) using the following sequences: miR16 sense: 5'-UAGCAGCACGUAAAUAUUGGCG-3'; N.C.sense: 5'-UUGUACUACACAAAAGUACUG-3'. The anti-cancer drug ADR was purchased from Wolsen Biotechnology (Xi'an, China). Rabbit polyclonal antibody specific to Bcl-2 was purchased from Santa Cruz Biotechnology (Santa Cruz, CA). Antibody specific to human sodium iodide symporter (hNIS), cleaved form of caspase3 and poly (ADP-ribose) polymerase (PARP) as well as β -actin were purchased from Abcam (Cambridge, UK). The terminal deoxynucleotidyl transferase-mediated dUTP nick end-labeling (TUNEL) cell apoptosis detection kit was provided by Beyotime Institute of Biotechnology (Haimen, China). All cell culture media and serum were purchased from Gibco (Grand Island, NY).

Cell culture

Human gastric cancer cell line SGC7901 and its multidrug resistant variant SGC7901/ADR were established and maintained in our laboratory as previously described. In brief, they were cultured in RPMI-1640 medium supplemented with 10% fetal calf serum and 100 unit penicillin and 100 mg/mL streptomycin (Invitrogen). To maintain the MDR phenotype, adriamycin (ADR) with final concentration of 0.5mg/ml was added to the culture medium.

SGC7901/ADR^{fluc} and NF/3XmiR16 SGC7901 were also established and cultured in our laboratory²⁰. Fluc (firefly luciferase reporter) gene is encoded by SGC7901/ADR^{fluc} cell lines. Once the luminescent substrate D-luciferin is added, SGC7901/ADR^{fluc} can exhibit bioluminescence signal that can be captured by particular imaging system. As to NF/3XmiR16 SGC7901, a dual expression vector was constructed by inserting the cDNA of

hNIS gene into the BamH and Age I restriction enzyme sites of a lentiviral vector GV260-Fluc-puro (Shanghai GeneChem, China) that encoding Fluc. After that, copies of complementary sequences against miR16 were inserted after the stop codon of the hNIS/Fluc gene. The constructed vector was used to infect SGC7901 cells, which resulted in NF/3XmiR16 SGC7901 cell line. In this cell line the Fluc fluorescence intensity and hNIS expression are reversely correlated with the intracellular miR16 level and can be used as an indirect index of miR16 intracellularly.

Preparation of PEG-coated Fe₃O₄ nanoparticles (MNPs)

Firstly, biocompatible Fe₃O₄ nanoparticles were synthesized as previously reported. Typically, 2.1 g of Fe(acac)₃ (6 mmol), 7.9 mL of oleylamine (24 mmol), and 24 g of amine terminated PEG (12 mmol) were dissolved in 100 mL of diphenyl ether solution. The solution was purged with nitrogen for 2 h to remove oxygen under mechanical stirring at 400 rpm. After being incubated at 80 °C for 4 h, the reaction mixture was quickly heated to reflux within 10 min and maintained at reflux for 30 min for monitoring the particle formation and growth. Ether was introduced to precipitate and isolate the resultant Fe₃O₄ nanocrystals out of the reaction mixture after it was cooled to room temperature. Then, the precipitate was re-dissolved in ethanol followed by addition of ether as precipitant. Typically, this purifying procedure was repeated for three cycles. By being re-dispersed in ethanol and subsequently precipitated with ether for three cycles, the PEG-coated Fe₃O₄ nanoparticles were purified and dissolved in either Milli-Q water or PBS for further experiments.

Preparation of Cy5.5 conjugated MNPs

Cy5.5 mono-NHS ester (2.25 mg), a commonly used fluorescent dye, dissolved in 250 μL of dimethyl sulfoxide (DMSO) was added slowly to 50mg of MNPs, which was dispersed in 50 ml of PBS. After being allowed to react on ice in the dark with vigorous stirring for 24 h, unreacted Cy5.5 was removed by gel filtration on Sephadex G-50. After labeling, the mixture was dialyzed using an 8.0 kDa molecular weight cut-off membrane (Spectrum Chemicals

& Laboratory Products, California, USA), followed by lyophilization. Finally, Cy5.5 was conjugated with the amino groups of PEG to allow *in vivo* tracking of MNPs distribution by fluorescence imaging. These resulting Cy5.5-conjugated MNPs were stored at 4 °C in the dark for further use.

Synthesis of miR16/MNPs

miRNA (purchased from Jima, China) was negatively charged and the surface of MNPs was positive charged. Therefore, miRNA and MNPs can be linked by electrostatic interaction. Briefly, miR16 was dissolved in Milli-Q water and then mixed with MNPs at room temperature for one hour. miR16/MNPs was characterized at 298.0 K via the dynamic light scattering (DLS) method using an instrument (Nano ZS, Malvern) equipped with a solid-state He₂Ne laser ($\lambda=633$ nm). The efficacy of the miRNA linked to MNPs was evaluated by agarose gel electrophoresis. The structure of ultimately synthesized miR16/MNPs conjugated with Cy5.5 was illustrated as Figure 1A.

Characterization of miR16/MNPs

TEM (transmitting electronic microscopy) images were acquired using a transmission electron microscope (JEM-100CXII) operating at an accelerating voltage of 100 kV. More than 400 quasi-spherical particles were measured for gaining the average equivalent area diameter of the MNPs. Magnetization measurements were obtained by using a vibrating sample magnetometer (VSM JDM-13, China). The hydrodynamic size of the samples was characterized at 298.0 K by DLS using an instrument (Nano ZS, Malvern) equipped with a solid-state He₂Ne laser ($\lambda=633$ nm). The organic content was measured by thermo gravimetry analysis (TG/DTA 6300, SII Nanotechnology Inc). The efficacy of the miRNA linked to MNPs was evaluated by agarose gel electrophoresis.

Determination of cell toxicity of MNPs by MTT

20,000 cells were plated into each well of 96-well flat-bottomed micro-titer plates. After 12 h incubation at 37 °C, medium containing MNPs (0 $\mu\text{g/ml}$ to 20 $\mu\text{g/ml}$) was added to the cells. After 48 h incubation, 20 μl of 5 mg/ml MTT

was introduced to each well and incubated for 4 h of exposure. The plates were centrifuged and medium was decanted. Cells were subsequently dissolved in 150 μ l DMSO with gentle shaking for 10 min at room temperature, followed by measurement of OD490 nm. Eight replicate wells were used in each point in each of three separate measurements.

Evaluation of intracellular uptake of MNPs

Intracellular uptake of MNPs by SGC7901 cells after co-culture *in vitro* was examined by Prussian blue staining and ICP-AES analyses were performed as previously reported. In brief, after incubation with 10 μ g/ml MNPs, 1×10^4 SGC7901 cells were washed with PBS and fixed for 15 minutes using 4% paraformaldehyde (Sigma-Aldrich). Then cells were washed with PBS and incubated with fresh prepared Pers' reagent (4% potassium ferrocyanide [Sigma-Aldrich]/12% HCl, 1:1, v/v) for 10 minutes. Then cells were washed three times with PBS, tumor tissue should be counterstained with neutral red (0.02%)(Sigma-Aldrich), and subsequently observed by an inverted optical microscope. ICP-AES was performed to quantify Fe to detect the dose of MNPs in the SGC7901 cells. After incubation with MNPs at 1, 2, 3, 5 hour, cells were washed with PBS and then dissolved in sulfuric acid and nitric acid. Then the concentration of Fe was measured by ICP-AES.

***In vitro* cells apoptosis assay**

5×10^5 SGC7901/ADR cells per well were seeded in 6-well plate. 24 h after co-culture with 100nM miR16/MNPs (200pmol miR16 loaded by 16.6 μ g MNPs in 2ml medium), cells were collected and drug sensitivity of which was evaluated by TUNEL and FACS. The SGC7901/ADR cells treated as aforementioned were fixed with 4% paraformaldehyde, rinsed with PBS, then permeabilized by 0.1% Triton X-100 for FITC end-labeling the fragmented DNA of the apoptotic cells using TUNEL cell apoptosis detection kit. The FITC-labeled TUNEL-positive cells were imaged under a fluorescent microscopy by using 488-nm excitation and 530-nm emission. For FACS assay, after

100nM miR16/MNPs co-cultured with 5×10^5 SGC7901/ADR cells for 24 h, cells were incubated with anti-cancer drugs ADR for 48 h. Then cells were harvested, and the Annexin V-FITC Apoptosis Detection Kit (BD Biosciences) was used for apoptosis assays. Cells were stained according to the manufacturer's protocol and sorted using a FACS sorter (BD Biosciences, La Jolla, CA, USA), and the data were analyzed using ModFit software (BD Biosciences).

***In vitro* bioluminescence imaging**

NF-3xmiR16/SGC7901 cells were constructed as described in our previous report²⁰. Before nanoparticles treatment, NF-3xmiR16/SGC7901 cells were seeded at 1×10^4 cells per well in a 24-well plate. After 24 h, miR16/MNPs and N.C./MNPs were co-cultured with NF-3xmiR16/SGC7901 cells. The concentration of miR16/MNPs or N.C./MNPs are from low to high (0nM, 25nM, 50nM, 75 nM and 100 nM). Typically, every 60pmol miR16 was loaded by 5 μ g MNPs. After 72 h, each well was washed with PBS. Then D-Luciferin (Xenogen Corporation, Massachusetts, USA) (0.5 mmol/L) was added immediately before assay. Bioluminescence signal was captured with an IVIS 100 Imaging system (Xenogen Corporation, Massachusetts, USA) and the intensity was analyzed using the Living Image software version 2.50.

Experimental protocol *in vivo*

SGC7901/ADR^{fluc} (5×10^6) were xenografted subcutaneously into the right shoulder of each female nude mouse aging 6-8 weeks (n=18). When the diameter of tumor reached around 0.5 cm, mice were divided into 3 groups randomly: group I (saline), group II (N.C./MNPs) and group III (miR16/MNPs). Saline, N.C./MNPs (5 mg/kg) or miR16/MNPs (5 mg/kg loading 1.0 nmol miR16) was intravenously injected via tail vein at day0, day3, day7, day10, day14, day17 and day21 post establishment of xenografted tumor model. ADR (2.5 mg/kg) was administered at day0, day7, day14 and day21 by intraperitoneal injection. Tumor volume ($V=AB^2/2$, where A is tumor length and B is tumor width) was calculated and BLI was acquired every week.

Bioluminescent imaging (BLI), fluorescent imaging (FI) and magnetic resonance imaging (MRI) of nude mice *in vivo*

After establishment of SGC7901/ADR^{fluc} xenografted tumor model, BLI was performed using IVIS 100 system in a serial of time points (day7, day14, day21 and day28) post nanoparticles injection. Bioluminescence signal was captured 5 min after intravenous injection of D-Luciferin (0.5 mmol/L) into mice under anesthesia by isoflurane. Bioluminescence and cy5.5 fluorescence signals were detected using IVIS 100 system.

MRI was analyzed by a 3-T MRI system (Siemens, Germany). In brief, the tumor-bearing mice were intravenously injected with MNPs (5 mg/kg), before and after injection for 24 h, MR imaging were conducted on a 3-T clinical MRI scanner.

Statistical Analysis

Results are expressed as mean \pm standard deviation (SD). SPSS17.0 (SPSS Inc., USA) and Prism 5.0 (GraphPad Software, USA) were used to perform the one-way analysis of variance (ANOVA). A two-tailed *P*-value <0.05 was considered significant.

Results

Characterization of MNPs

MNPs were synthesized by thermal decomposition. A representative transmission electron microscopy (TEM) image of the resulting biocompatible Fe₃O₄ nanoparticles is shown in Figure 1B with a size range of 12.4 \pm 1.6nm. Figure 1C reveals that the average hydrodynamic size of the MNPs is about 48.6 nm. The organic content of the current MNPs sample was around 65.3% (Figure 1D). Fe₃O₄ nanocrystals are superparamagnetic and present a

saturation magnetization of 63.5 emu/g at 25 °C (Figure 1E).

Cytotoxicity assay of MNPs

Cell viability studies were performed by incubating MNPs with SGC7901 cells at different concentrations and assaying the cell metabolic activity after 24 h. Figure 2A showed the low toxicity of MNPs even at the highest concentration of 20 µg/ml. The excellent biocompatibility of the MNPs may be attributed to the introduction of biocompatible PEG into the MNPs.

Intracellular uptake of MNPs

Prussian blue staining and ICP-AES analyses were conducted to determine the fate of MNPs after incubation with SGC7901 cells *in vitro* and showed that MNPs began to enter cells after 1 h of co-culture and reached the peak at 3 h (Figure 2B and C). The concentration of iron per cell decreased modestly at 5 h, which may be caused by exocytosis.

Characterization of miR16/MNPs

TEM was used to assess the size of miR16/MNPs. After MNPs (10 µg) coupled with 10, 20 30 and 40 pmol miR16, the produced miR16/MNPs didn't show significant variation of size (Figure 3A and B). The reasonable increase of the hydrodynamic size strongly suggested that miR16 was effectively loaded onto the MNPs via electrostatic interaction. Zeta-potential of MNPs was measured as a range of 6.65 ± 0.78 mV, while changing to -7.6 ± 0.21 mV after coupled with miR16 (Figure 3C). To determine the stability of miR16/MNPs, we measured the hydrodynamic size of miR16/MNPs at 0 h, 12 h, 24 h and 48 h. Results showed miR16/MNPs remained stable at 48 h (Figure 3D). In addition, we examined miRNA binding ability using agarose gel electrophoresis. MNPs were mixed with miR16 at various weight ratios and then incubated for 60 min to form polyelectrolyte complexes. As Figure 3E showed, the content of free miRNA gradually decreased with increasing weight ratio, indicating the

successful formation of charge-neutralized polyelectrolyte complexes. In addition, Figure S2A shows the photographs of miR16/MNPs in various media such as PBS, saline, cell medium and serum, which revealed the good water solubility and stability of miR16/MNPs. After the centrifugation filtration, no noticeable miRNA was detected in the removed solution by agarose gel electrophoresis analysis (Figure S2B), indicating sound conjugation of miR16 with MNPs without significant detachment even in serum.

miR16/MNPs increased the functional expression of miR16 in SGC7901 cells

NF/3XmiR16 SGC7901 cells were employed to assess the expression of miR16 in SGC7901 cells post transfection. After co-cultured with miR16/MNPs, SGC7901 cells exhibited dramatically decreased luminescence intensity, compared with N.C./MNPs treatment (Figure 4A and B), indicating that miR16/MNPs are able to increase the expression of miR16 in NF/3Xmir16 SGC7901 cells, which was also confirmed by the reduction of hNIS expression (Figure 4C and D). Then we detected the expression of Bcl-2, the endogenous target gene of miR16, which was significantly reduced in miR16/MNPs group (Figure 4E and F). These results combined indicate successful intracellular introduction of miR16/MNPs and this introduction might increase the functional level of miR16 in targeted cells.

miR16/MNPs increased the sensitivity of SGC7901/ADR cells to ADR *in vitro*

TUNEL, MTT and FACS assay were performed to assess the sensitivity of SGC7901/ADR cells to ADR after treated with miR16/MNPs or N.C./MNPs for 24 hours. TUNEL staining showed that after co-culture with nanoparticles, miR16/MNPs group showed higher apoptotic rate (24.8%) than both N.C./MNPs treated group (14.5%) and control group (12.4%) (Figure 5A and B). MTT test demonstrated that the IC_{50} of ADR in miR16/MNPs treated cells is 2.0 mg/ml, significantly lower than that of control or N.C./MNPs treated cells (Figure 5C). FACS assay also showed much more apoptotic cells in miR16/MNPs group than other two groups (Figure 5D). Furthermore, We

examined the effect of miR16/MNPs on caspase3 activation by western blot analysis. As shown in Figure 5E, treatment of SGC7901 cells with miR16/MNPs led to drastic activation of caspase3, as evidenced by increased cleaved-caspase3 level (Figure 5F). We also detected the effect of miR16/MNPs on the death substrate poly (ADP-ribose) polymerase (PARP), which is capable of mediating DNA fragmentation during apoptosis upon switching from pro- to active forms by cleaved caspase3. Our results revealed that activation of caspase3 correlated with activation and cleavage of PARP (Figure 5G). All those data suggested that miR16/MNPs could sensitize SGC7901/ADR cells to ADR induced apoptosis.

miR16/MNPs accumulated passively in tumor area *in vivo*

IVIS 100 Imaging system and a 3-T MRI system were employed to acquire optical imaging signal and MRI signal, respectively. MNPs were labeled with Cy5.5 NHS ester for *in vivo* imaging. Before injection, successful Cy5.5/MNPs connection was confirmed by NIR (near infra-red) optical imaging. As Figure 6A and 6B showed, similar fluorescence intensity was produced by cy5.5 and cy5.5/MNPs while no signal were generated by unmodified MNPs. Tumor uptake of cy5.5/MNPs was detected by NIR optical imaging and MRI *in vivo* as well as Prussian blue staining *ex vivo*. Both MRI (left panel) and fluorescent imaging (middle panel) modalities showed enrichment of MNPs in tumor site (Figure 6C), which was also confirmed by Prussian blue staining (Figure 6D). Those data indicated miR16/MNPs were able to achieve targeted accumulation in tumor site after systemic administration, which might be attributed to EPR effect. Meanwhile, the BLI imaging confirmed the successful establishment of SGC7901/ADR^{fluc} tumor with overexpression of Fluc gene, which can generate strong bioluminescence signal (right panel; Figure 3C). Moreover, to evaluate the toxicity of our synthesized miR16/MNPs *in vivo*, we harvested the major organs of miR16/MNPs treated mice for histology analysis, including heart, liver, spleen and kidney. Compared with normal tissue, no noticeable damage of those critical organs was observed from H&E staining (Figure S1), indicating the feasibility of systemic use of miR16/MNPs.

miR16/MNPs increased the sensitivity of SGC7901/ADR cells to ADR *in vivo*

Tumor bearing mice were injected with ADR (2.5 mg/kg, IP) twice a week by intraperitoneal injection. miRNA/MNPs containing 1nmol miRNA or equivalent amount of N.C/MNPs were injected once every week via tail vein. Tumor bioluminescence imaging and tumor volume measurement were performed every week. As shown in Figure 7A and 7B, the bioluminescence signal intensity of tumor decreased over time in miR16/MNPs group while increased in control or N.C/MNPs group. At day 28, compared to control or N.C/MNPs group, the luciferase signal in miR16/MNPs group was significantly lower, indicating death of tumor cells and reduction of tumor size post miR16/MNPs administration. Tumor volume measurement also confirmed tumor size reduction in miR16/MNPs group (Figure 7C). Moreover, we also collected the tumor slice to further confirm the effect of systemic use of miR16/MNPs on cancer cell apoptosis by TUNEL staining. As Figure S4 showed, the amount of apoptotic nuclei increased remarkably within cancer tissue after miR16/MNPs administration, indicating induced apoptosis of cancer cells *in vivo* by miR16/MNPs. Taken together, our results indicated that miR16/MNPs increased the sensitivity of SGC7901/ADR cells to ADR *in vivo*.

Discussion

Drug resistance is one of the most common causes of chemotherapy failure in treatment of gastric cancer. Multi-drug resistance (MDR) in cancer refers to the capacity of cancer cells to survive or become resistant to treatment of a wide variety of anti-tumor medications. Mechanisms of MDR include decreased uptake of drugs, reduced intracellular drug concentration by activation of the efflux transporters, modifications in cellular pathways by altering cell cycle checkpoints, increased metabolism of drugs, induced emergency response genes to impair apoptotic pathways and altered DNA repair mechanisms. Despite of the discovery of multiple new gene/protein

expression signatures or factors associated with drug resistance by high throughput “-omics” technologies, little clinical success has been achieved in reversing the MDR via traditional strategy such as the development of ATP-binding cassette transporter inhibitors²¹.

It has been reported that changes in miRNA expressions were involved in drug resistance and modulation of miRNA expression could partially overcome drug resistance and pronouncedly improve the anti-tumor activity of certain drugs²². So far, many miRNAs are found involved in the drug resistance of gastric cancer³. In our previous work, overexpression of miR15b or miR16 could sensitize SGC7901/VCR cells to anticancer drugs by targeting Bcl-2 in human gastric cancer cells. Moreover, overexpression of miR15b or miR16 could sensitize SGC7901/VCR cells to VCR-induced apoptosis. Proving that in theory, it is possible to reverse MDR in gastric cancer cells⁶. However, the manipulation of miR16 expression via a viral delivery system is hampered by safety concerns as to its clinical application.

In the past few years, nanoparticles have been emerging as particularly promising gene therapy vectors. Due to their controlled release characteristics and biocompatibility, nanoparticles conjugated with miRNA could release their payload over extended periods of time, making them potential candidates for miRNA delivery to MDR cancer tissue. Traditional nanoprobe for miRNA imaging and delivery have several drawbacks, including sophisticated synthetic processes, limited intensity for detection *in vivo*, low efficacy upon systemic administration and potential toxicity to normal tissue^{23, 24}. PEG-coated Fe₃O₄ nanoparticle carrying miR16 (miR16/MNPs) we synthesized here exhibited its own superiorities. Firstly, we employed the thermal decomposition method to develop a simple route for synthesizing water-soluble and biocompatible magnetic nanoparticles with PEG modification via a “one-pot” reaction¹⁵. Secondly, surface modification of nanoparticles with PEG prolongs the blood half-life and enhances the bioavailability of miR16/MNPs, owing to increased retention of the complex in serum without affecting the silencing ability of miRNA portion^{25, 26}. Prolonged silencing *in vivo* by PEGylated reagent could lower the doses required for

effective therapy, reducing dosage-dependent adverse effects. Moreover, the main component of MNPs is iron oxide, which is biodegradable and bears minimal toxicity²⁷. Thirdly, relative large Fe₃O₄ nanoparticles led to strong MR contrast enhancement effect without compromising the loading capacities for both miR16 and dye Cy5.5, resulting in strong silencing ability as well as decent fluorescence imaging signal. Last but not least, it has been well-documented that nanoparticle can be targeted to tumor with high vascular permeability through EPR (enhanced permeability and retention) effect, achieving higher drug concentration at the target site. This effect can markedly increase the local concentration of miR16/MNPs and improve the efficacy of miR16 delivery.

In our study, miR16/MNPs accumulation in tumor was demonstrated by both *in vivo* and *in vitro* examination. The delivery efficiency was first evaluated by bioluminescence intensity measurement *in vitro*. In cultured NF/3Xmir16 SGC7901 cells, miR16/MNPs treatment significantly reduced the intensity of bioluminescence, suggesting successful introduction of miR16. The introduction of miR16 was further confirmed by down-regulation of Bcl-2, target gene of miR16 as discovered in our previous study. Targeting of the miRNA payload to the tumor *in vivo* is vital to the success of nanoparticle based therapy. We injected miR16/MNPs to mice with SGC7901/ADR^{fluc} cells xenografted subcutaneously. The advent of molecular imaging techniques allows the noninvasively visualization of many pathophysiological processes in living subjects at molecular level. Nanoparticles could be traced *in vivo* by molecular imaging via their intrinsic character or by fluorescent dye and radioactive isotope attached to the particles^{28, 29}. In our research, we took advantage of the magnetic property of iron oxide core and conjugated fluorescent dye on the surface of nanoparticles to achieve both MR imaging and optical imaging simultaneously *in vivo*. The accumulation of miR16/MNPs in the tumor area was evidenced by strong fluorescence signal generated by cy5.5 linked on the surface and MRI signal generated by magnetic Fe₃O₄ core.

Apart from unsatisfying treatment outcome, traditional approach often leads to inaccurate evaluation of disease progression and therapeutic effect for lack of ideal monitoring tool. Consequently, combing functional molecular

imaging with elaborately designed nanoparticles is of great importance and able to facilitate the advancement of cancer diagnosis and therapy due to the advantages of favorable pharmacodynamics, target specificity and quantitative nature³⁰. In our study, multifunctional Fe₃O₄ nanoparticles loaded with miR16 produced a remarkable effect on sensitizing SGC7901 cells to ADR. However, some previous studies reported that magnetic iron oxide nanoparticles were able to induce drug sensitivity especially to another ADR-class drug, doxorubicin (DOX) in magnetic field³¹. This phenomena could be attributed to the increased DOX release and/or the hyperthermia effect of high frequency magnetic field³². To exclude the possible effect caused by magnetic field, we employed MNPs without loading miR16 as the negative control in our work and our data demonstrated that MNPs alone did not lead to noticeable effect on sensitizing SGC7901 cells to ADR, compared with blank control. However, we think it would be very interesting to investigate whether MNP plays synergistic role with miR16 in our future work. Besides, EPR effect and PEG modification of miR16/MNPs guaranteed the good biocompatibility and favorable therapeutic effect *in vivo*, which was supported by reduced tumor volume as well as decreased bioluminescence signal in tumor area dynamically monitored by BLI imaging. Meanwhile, we linked cy5.5 to MNPs, which has the potential to allow *in vivo* tracking by both MRI and fluorescent imaging at the same time, thus comprehensive theranostic evaluation of gastric cancer might be achieved .

Although results showed significant suppression of tumor growth, more effort are required to further understand the *in vivo* behaviors and improve both diagnostic and therapeutic efficacy of miRNA-loaded MNPs, including determine the proper dose and duration of particles delivery using larger cohort of animals; synthesis of new nanoparticles conjugated with specific antibody in order to achieve active targeting; and selecting other potent miRNAs to obtain better effect of cancer therapy.

In summary, we developed and characterized a new MNP based carrier for tumor-targeted delivery of miR16 in tumor-bearing mice, which can be well tolerated with little toxicity. Our results showed the successful delivery of

miRNA to the tumor tissue using MNPs both *in vitro* and *in vivo*, which was confirmed by multiple imaging modalities including fluorescence, MRI and bioluminescence imaging. Moreover, miR16/MNPs hold great potential for increasing the sensitivity of gastric cancer cells to ADR, the process of which could be dynamically monitored and accurately evaluated by molecular imaging approach. Our work suggests the great promise of using miR16/MNPs in therapeutic application for treating drug-resistant gastric cancer.

Acknowledgment

This work was supported by National Nature Science Foundation of China (No.81090274, No.81270168, No.81325009, No.81227901 and No.81400366), Innovation Team Development Grant by China Department of Education (IRT1053), National Basic Research Program of China (2012CB518101).

References

1. D. Zhang and D. Fan, *Future Oncol*, 2010, **6**, 527-537.
2. R. Wong and D. Cunningham, *Ann Oncol*, 2009, **20**, 605-608.
3. L. Hong, Z. Yang, J. Ma and D. Fan, *Curr. Drug.Targets*, 2013, **14**, 1118-1127.
4. Q. Ma, X. Wang, Z. Li, B. Li, F. Ma, L. Peng, Y. Zhang, A. Xu and B. Jiang, *Oncol Rep*, 2013, **29**, 1652-1658.
5. M. Hao, L. Zhang, G. An, W. Sui, Z. Yu, D. Zou, Y. Xu, H. Chang and L. Qiu, *J. Hematol. Oncol*, 2011, **4**, 37.
6. L. Xia, D. Zhang, R. Du, Y. Pan, L. Zhao, S. Sun, L. Hong, J. Liu and D. Fan, *Int. J. Cancer*, 2008, **123**, 372-379.

7. T. Behnke, J. E. Mathejczyk, R. Brehm, C. Wurth, F. R. Gomes, C. Dullin, J. Napp, F. Alves and U. Resch-Genger, *Biomaterials*, 2013, **34**, 160-170.
8. S. Cui, D. Yin, Y. Chen, Y. Di, H. Chen, Y. Ma, S. Achilefu and Y. Gu, *ACS nano*, 2013, **7**, 676-688.
9. C. H. Fan, C. Y. Ting, H. J. Lin, C. H. Wang, H. L. Liu, T. C. Yen and C. K. Yeh, *Biomaterials*, 2013, **34**, 3706-3715.
10. H. Maeda, H. Nakamura and J. Fang, *Adv Drug Deliv Rev*, 2013, **65**, 71-79.
11. Y. Zhang, L. Peng, R. J. Mumper and L. Huang, *Biomaterials*, 2013, **34**, 8459-8468.
12. R. Shrestha, M. Elsabahy, S. Florez-Malaver, S. Samarajeewa and K. L. Wooley, *Biomaterials*, 2012, **33**, 8557-8568.
13. K. A. Whitehead, J. Matthews, P. H. Chang, F. Niroui, J. R. Dorkin, M. Severgnini and D. G. Anderson, *ACS nano*, 2012, **6**, 6922-6929.
14. H. C. Huang, S. Barua, G. Sharma, S. K. Dey and K. Rege, *J. Control Release*, 2011, **155**, 344-357.
15. G. Yu, J. Li, W. Yu, C. Han, Z. Mao, C. Gao and F. Huang, *Adv Mater*, 2013, **25**, 6373-6379.
16. J. Chen, M. Shi, P. Liu, A. Ko, W. Zhong, W. Liao and M. M. Xing, *Biomaterials*, 2014, **35**, 1240-1248.
17. R. Qiao, Q. Jia, S. Huwel, R. Xia, T. Liu, F. Gao, H. J. Galla and M. Gao, *ACS nano*, 2012, **6**, 3304-3310.
18. Q. Jia, J. Zeng, R. Qiao, L. Jing, L. Peng, F. Gu and M. Gao, *J. Am. Chem. Soc*, 2011, **133**, 19512-19523.
19. S. Liu, Y. Han, R. Qiao, J. Zeng, Q. Jia, Y. Wang, and M. Gao, *J. Phys. Chem. C*, 2010, **114**, 21270-21276.
20. F. Wang, X. Song, X. Li, J. Xin, S. Wang, W. Yang, J. Wang, K. Wu, X. Chen, J. Liang, J. Tian and F. Cao, *PLoS one*, 2013, **8**, e61792.
21. H. Lage, *Cell. Mol. Life. Sci*, 2008, **65**, 3145-3167.
22. S. Husted, R. Sokilde, L. Rask, S. Cirera, P. K. Busk, J. Eriksen and T. Litman, *Mol Pharm*, 2011, **8**, 2055-2062.
23. H. C. Huang, S. Barua, G. Sharma, S. K. Dey and K. Rege, *J. control release*, 2011, **155**, 344-357.

24. H. Song, R. He, K. Wang, J. Ruan, C. Bao, N. Li, J. Ji and D. Cui, *Biomaterials*, 2010, **31**, 2302-2312.
25. Q. Jia, J. Zeng, R. Qiao, L. Jing, L. Peng, F. Gu and M. Gao, *J. Am. Chem. Soc.*, 2011, **133**, 19512-19523.
26. S. M. Moghimi, A. C. Hunter and J. C. Murray, *Pharmacol Rev.*, 2001, **53**, 283-318.
27. S. Laurent and M. Mahmoudi, *Int. J. Mol. Epidemiol. Genet.*, 2011, **2**, 367-390.
28. P. Chandrasekharan, D. Maity, C. X. Yong, K. H. Chuang, J. Ding and S. S. Feng, *Biomaterials*, 2011, **32**, 5663-5672.
29. J. Gao, K. Chen, R. Luong, D. M. Bouley, H. Mao, T. Qiao, S. S. Gambhir and Z. Cheng, *Nano letters*, 2012, **12**, 281-286.
30. F. F. Teng, X. Meng, X. D. Sun and J. M. Yu, *Int. J. Nanomed.*, 2013, **8**, 3703-3713.
31. H. Oliveira, E. Perez-Andres, J. Thevenot, O. Sandre, E. Berra and S. Lecommandoux, *J. control release*, 2013, **169**, 165-170.
32. M. Rahimi, S. Kilaru, G. E. Sleiman, A. Saleh, D. Rudkevich and K. Nguyen, *J. Biomed. Nanotechnol.*, 2008, **4**, 482-490.

Figure legend:

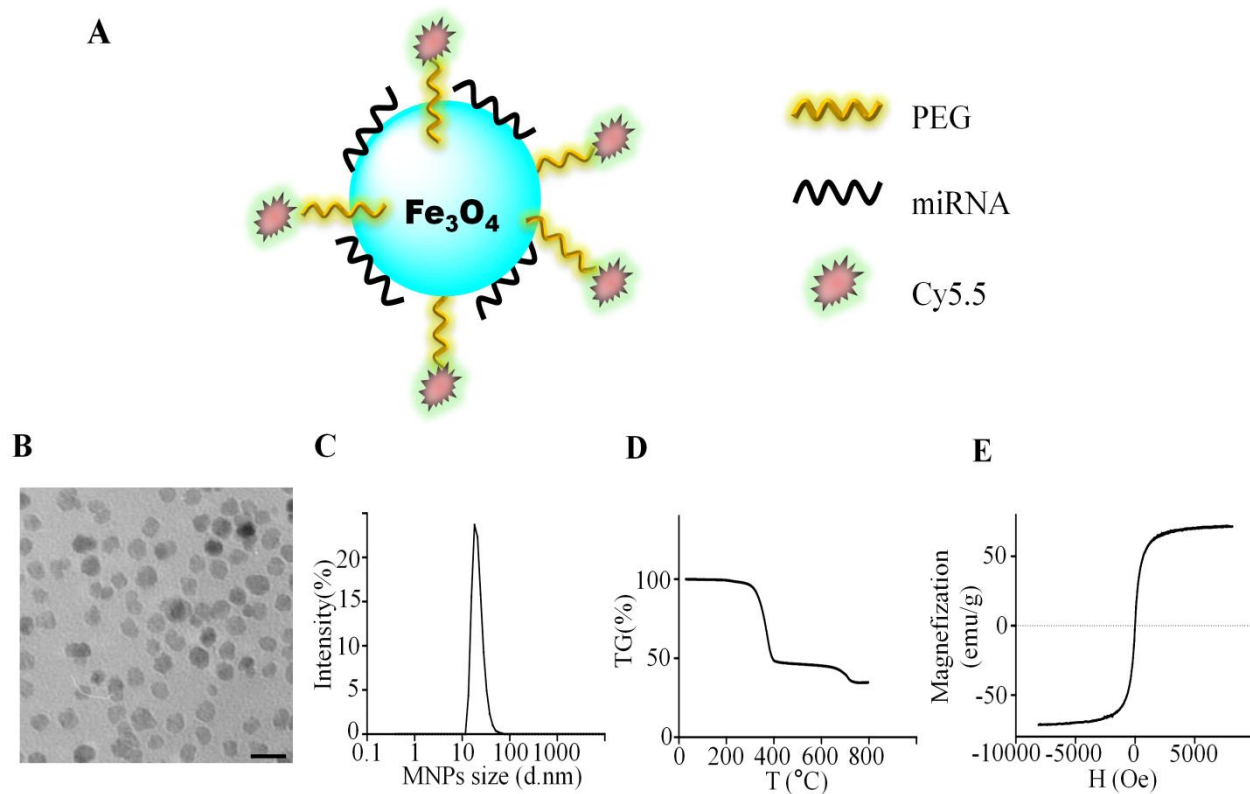


Figure.1. (A) Schematic illustration of miR16/MNPs. (B) Morphological observations of MNPs. Scale bar = 50 nm. (C)

Particle size distribution of MNPs. (D) The organic content of MNPs. (E) Magnetization of MNPs.

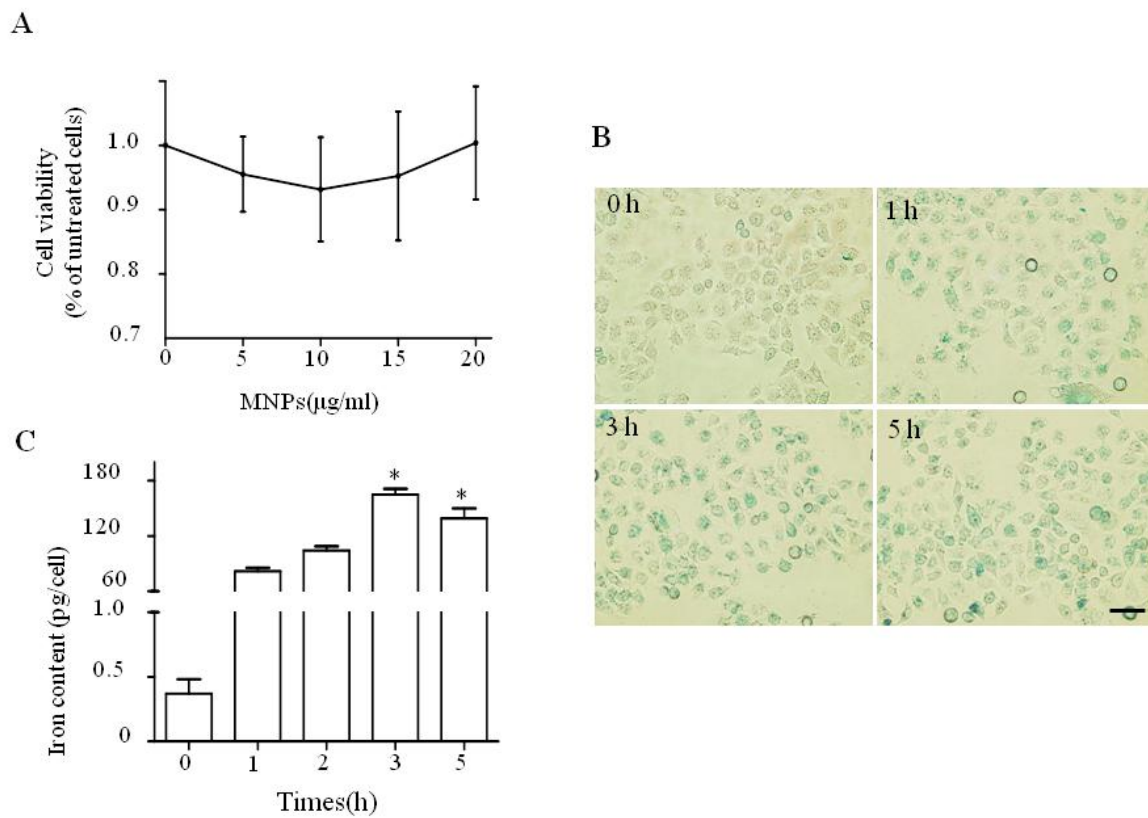


Figure.2. (A) Cytotoxicity of MNPs to SGC7901 cells by MTT assay. (B) Microscope images of Prussian blue dye stained SGC7901 cells. The iron in the cells was stained blue. (C) Iron accumulation in SGC7901 cells detected by ICP AES analysis. * $P < 0.05$ compared with 2 h.

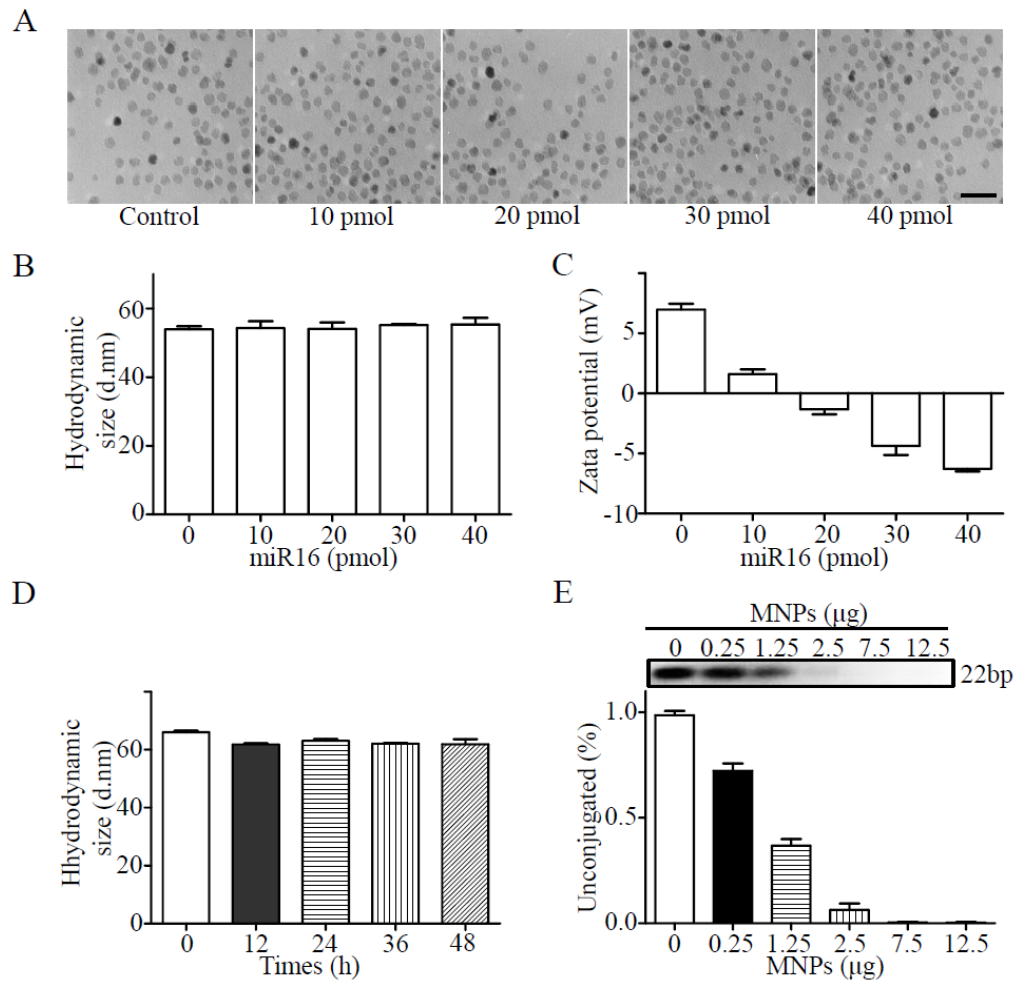


Figure.3. (A) Morphological observations of miRNA/MNPs. Scale bar = 50 nm. (B) And (C) After 10µg MNPs were connected to 0, 10, 20, 30 and 40 pmol miRNA, the hydrodynamic size (B) and Z-potential (C) of the samples were characterized at 298.0 K by a DLS using an instrument. (D) The hydrodynamic size of miRNA/MNPs was characterized at 0, 12, 2, 36 and 48 hours. (E) Agarose gel electrophoresis for analysis of unconjugated miR16/MNPs ratio. Lane 1:60pmol miR16, Lane 2: 60pmol miR16 and 0.25µg MNPs, Lane 3: 60pmol miR16 and 1.25µgMNPs, Lane 4: 60pmol miR16 and 2.5µg MNPs, Lane 5: 60pmol miR16 and 7.5µg MNPs, Lane 6: 60pmol miR16 and 12.5µg MNPs.

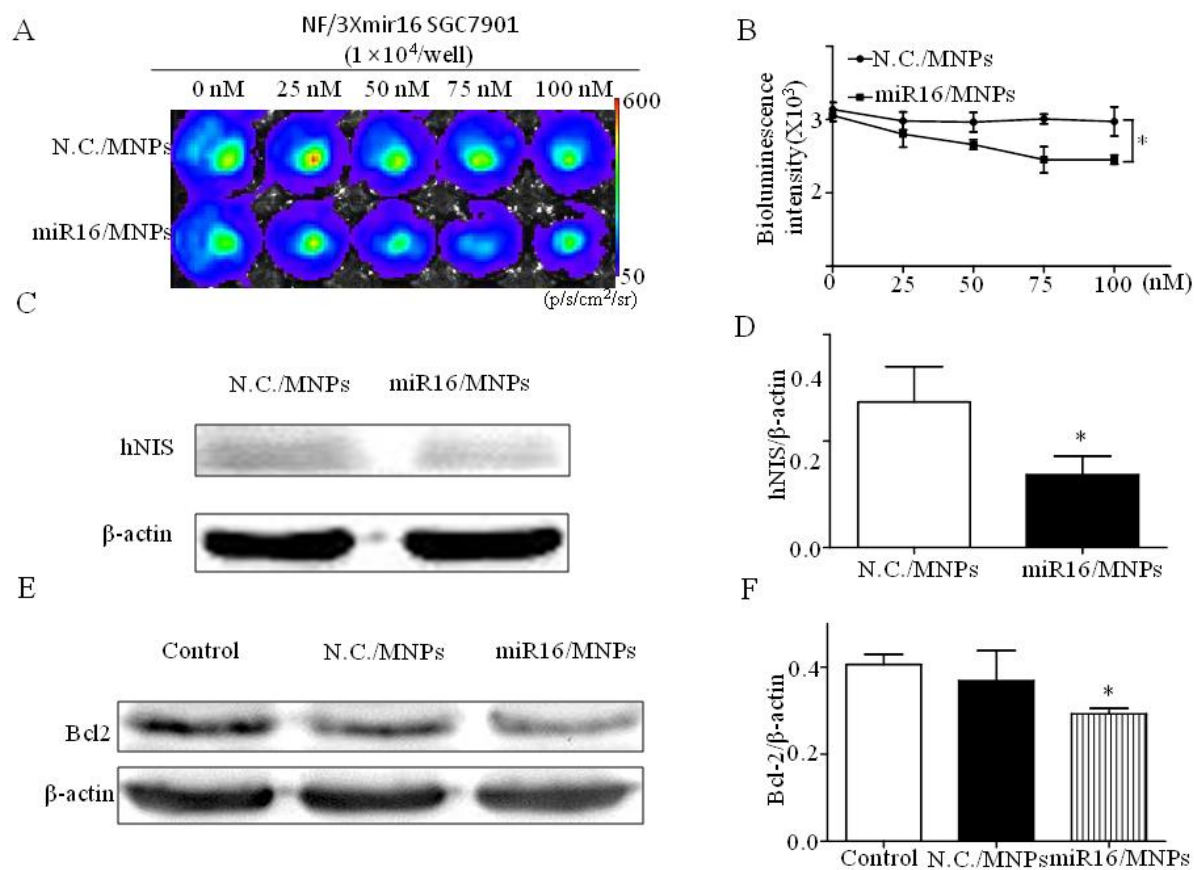


Figure 4. (A) Representative bioluminescence images of NF/3Xmir16 SGC7901 cells treated by miR16/MNPs or N.C./MNPs (N.C. means negative control miRNA) *in vitro*. (B) Statistic analysis of BLI signals intensity in different groups. Representative western blot images (C) and semiquantification (D) of hNIS expression after NF/3Xmir16 SGC7901 cells treated by miR16/MNPs or N.C./MNPs. Representative western blot images (E) and semiquantification (F) of Bcl-2 expression after NF/3Xmir16 SGC7901 cells treated by miR16/MNPs or N.C./MNPs. * $P < 0.05$ compared with N.C./MNPs group.

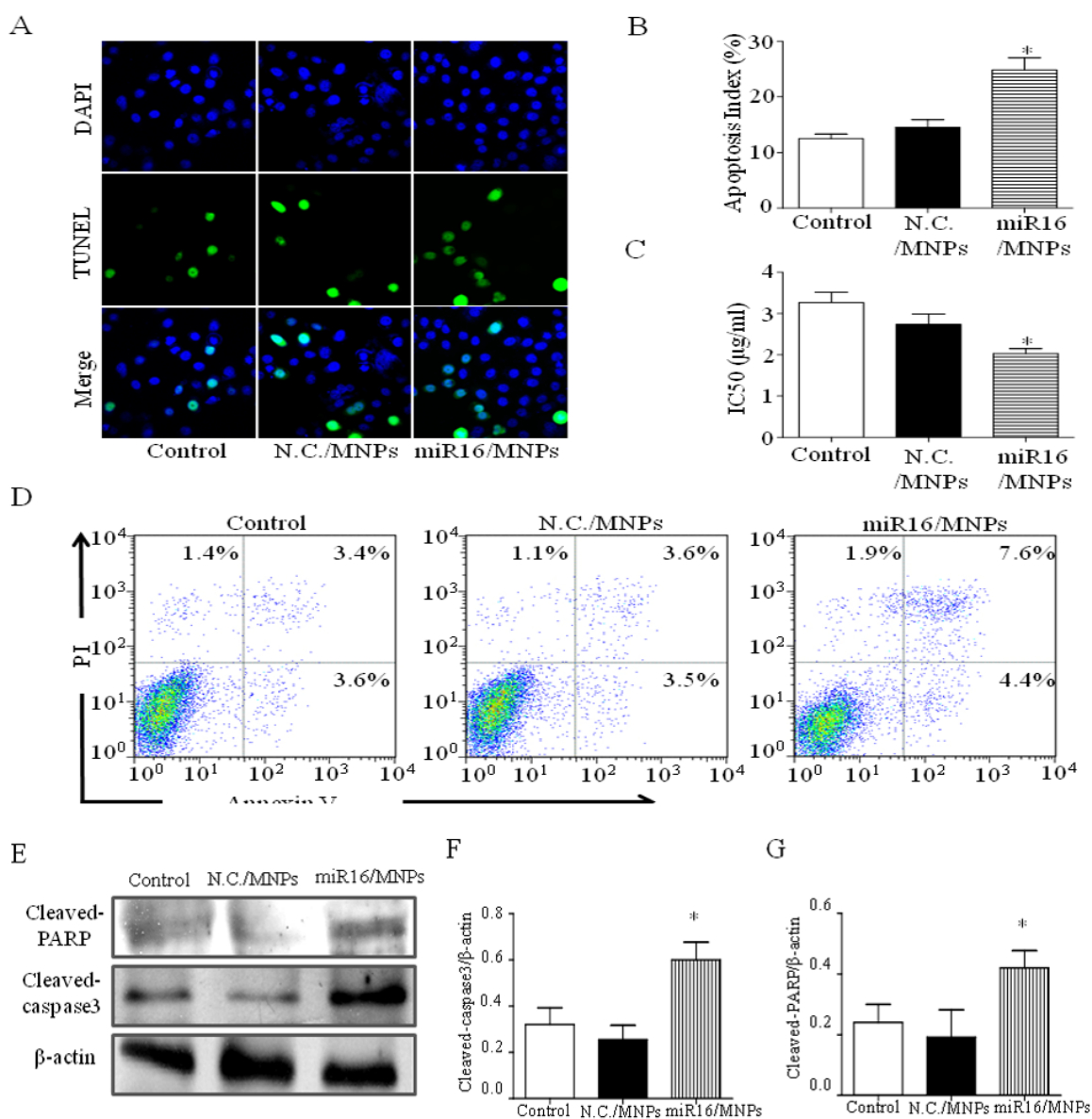


Figure 5. (A) and (B) Apoptotic cells were detected by TUNEL staining. (C) IC₅₀ of ADR in SGC7901/ADR cell lines after treated with N.C./MNPs or miRNA/MNPs. (D) Apoptotic cells were detected by FACS assay. Representative western blot images (E) and semiquantification of Cleaved-caspase3 expression (F) and Cleaved-PARP expression (G) after NF3/miR16 SGC7901 cells treated by miR16/MNPs or N.C./MNPs. **P*<0.05 compared with **P*<0.05 compared with N.C./MNPs group.

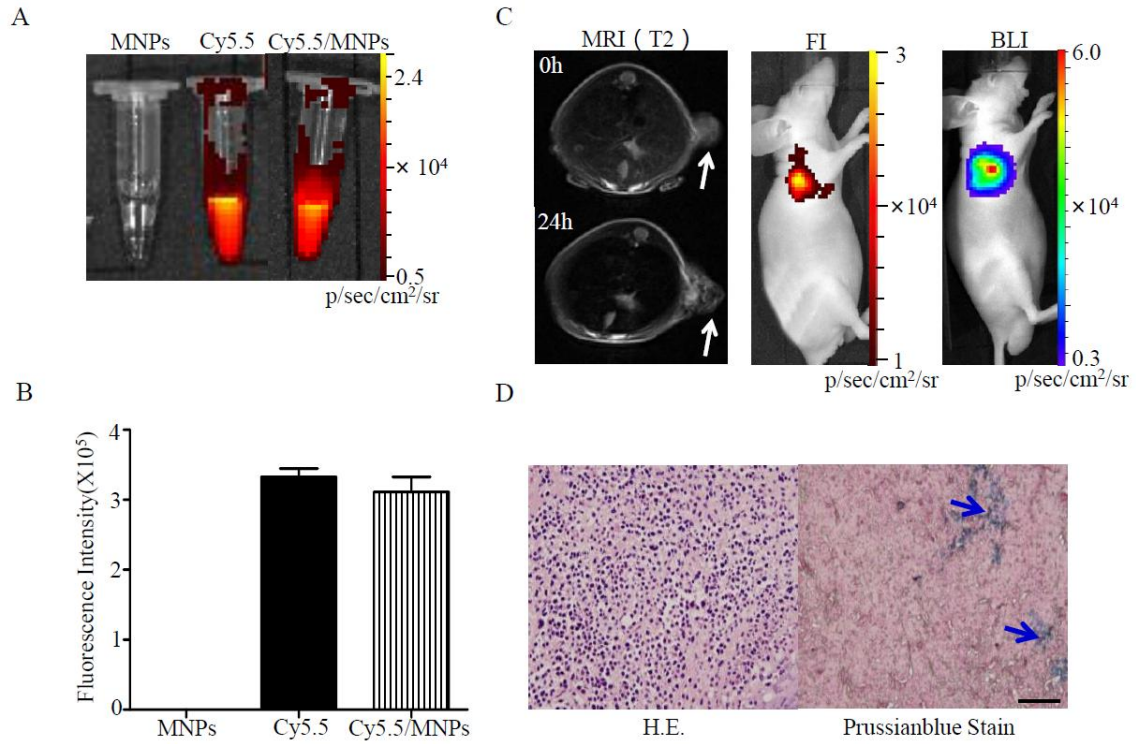


Figure.6. (A) Representative fluorescence images of of MNPs, cy5.5 and cy5.5/MNPs. (B) Statistic analysis of fluorescence signal intensity in different groups. (A) And (B) Fluorescence imaging of MNPs, cy5.5 and cy5.5/MNPs. (C) Distribution of cy5.5/MNPs after injected was detected by MRI, bioluminescence imaging and fluorescence imaging. (D) H&E and Prussian blue staining of cancer tissue. Magnification 40X; scale bar = 500 μ m

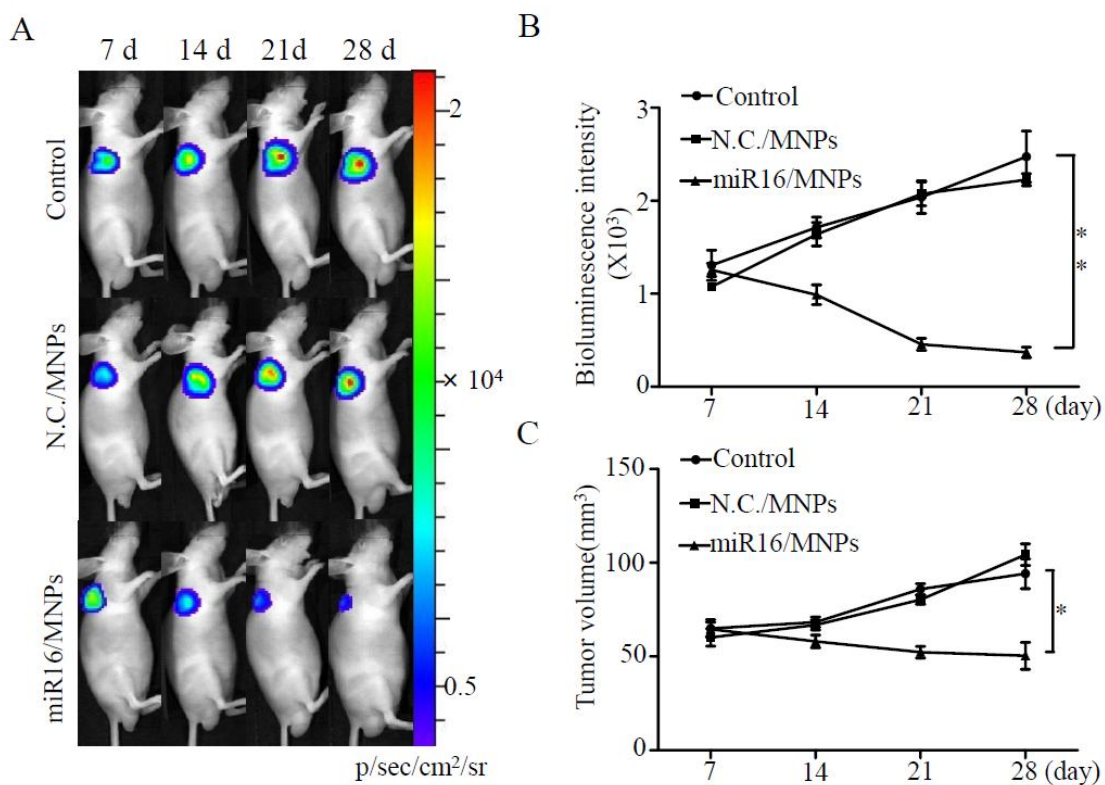


Figure.7. (A) Representative bioluminescence images of SGC7901/ADRfluc tumor in a serial of time points (day7, day14, day21 and day28) after treated with miR16/MNPs or N.C./MNPs *in vivo*. (B) Statistic analysis of BLI signals intensity in different groups. (C) Tumor volume measurement of different groups in a serial of time points (day7, day14, day21 and day28). n=6, * $p < 0.05$ compared with the control group